5654 *Chem. Mater.* **2009,** *21,* 5654–5663
DOI:10.1021/cm902181n

CHEMISTRY OF MATERIALS
Article

Highly Scattering, Surface-Enhanced Raman Scattering-Active, Metal Nanoparticle-Coated Polymers Prepared via Combined Swelling−Heteroaggregation

Jung-Hyun Lee, Mahmoud A. Mahmoud,[†] Valerie B. Sitterle,[‡] Jeffrey J. Sitterle,[‡] and J. Carson Meredith*

School of Chemical & Biomolecular Engineering, Georgia Institute of Technology, 311 Ferst Drive, Atlanta, Georgia 30332-0100, [†]School of Chemistry and Biochemistry, Georgia Institute of Technology, 901 Atlantic Drive, Atlanta, Georgia 30332-0400, and [‡]Georgia Tech Research Institute, Georgia Institute of Technology, 250 14th Street NW, Atlanta, Georgia 30332-0817

Received July 17, 2009. Revised Manuscript Received October 22, 2009

We report on a combined swelling−heteroaggregation (CSH) method for preparation of highly scattering, metal nanoparticle(NP)-coated polystyrene (PS) latex beads. This methodology is a facile and relatively benign single-step process for preparation of metal-coated dielectrics for applications in biomedical imaging, sensors, photonics, electronics, and surface-enhanced Raman scattering (SERS). A range of NPs with different sizes (30, 60, and 80 nm), chemistries (gold and silver), and shapes (sphere and cube) were successfully coated on the PS beads by using the CSH procedure. Homogeneous and dense metal coatings on the PS beads were obtained by the addition of tetrahydrofuran (THF) to an aqueous cosuspension of polyvinyl pyrrolidone (PVP) capped-metal NPs and 10 μm PS beads. Composite beads were stable with no loss of the NP coating during long-term (15 months) deionized (DI) water storage. The coating morphology, metal coverage, and optical properties of the composite beads were tunable by simple adjustments in THF and NP compositions as well as the NP chemistry, shape, and size. Dark field microscopy and UV−vis microspectroscopy of single beads showed highly enhanced scattering and tunable optical characteristics. Raman spectroscopy was used to confirm the SERS activity of the composite beads.

Introduction

Many applications involving metal nanoparticles (NPs) require their impregnation into a carrier particle (CP), often a submicrometer- to micrometer-sized polymer bead. Polymer CPs serve as supports, to passivate or protect the particles from the environment, to prevent leaching of NPs, and to facilitate transport of heat and mass. The assembly of such NP−CP constructs requires control over NP loading and distribution within the CP.

These metal NP−CP composite materials have attracted intense interest in recent years due to applications in electronics,[1,2] photonics,[3−6] medical imaging,[7,8] drug delivery,[9,10] immunoassays,[9,11−13] catalysis,[14] and surface-enhanced Raman scattering (SERS).[15,16] Gold (Au) and silver (Ag) NPs have been used widely due to their desirable optical, electronic, and biocompatibility properties. In particular, Au and Ag NPs are attractive for imaging applications because their resonance wavelengths can be tuned precisely over a broad range by controlling particle size and shape.[17] Metallic nanoshells, consisting of a dielectric core covered with a thin (<20 nm) shell of metal, exhibit a plasmon resonance that is a function of the core radius-to-shell thickness ratio.[18−20] Highly

*Corresponding author. E-mail: Carson.Meredith@chbe.gatech.edu. Tel.: +1-404-385-2151.

(1) Lee, J. H.; Kim, D. O.; Song, G. S.; Lee, Y.; Jung, S. B.; Nam, J. D. *Macromol. Rapid Commun.* **2007**, *28*, 634.
(2) Lee, J. H.; Oh, J. S.; Lee, P. C.; Kim, D. O.; Lee, Y.; Nam, J. D. *J. Electron. Mater.* **2008**, *37*, 1648.
(3) Kityk, I. V.; Ebothe, J.; Fuks-Janczarek, I.; Umar, A. A.; Kobayashi, K.; Oyama, M.; Sahraoui, B. *Nanotechnology* **2005**, *16*, 1687.
(4) Kubo, S.; Gu, Z. Z.; Tryk, D. A.; Ohko, Y.; Sato, O.; Fujishima, A. *Langmuir* **2002**, *18*, 5043.
(5) Li, M. J.; Zhang, H.; Zhang, J. H.; Wang, C. L.; Han, K.; Yang, B. *J. Colloid Interface Sci.* **2006**, *300*, 564.
(6) Rogach, A.; Susha, A.; Caruso, F.; Sukhorukov, G.; Kornowski, A.; Kershaw, S.; Mohwald, H.; Eychmuller, A.; Weller, H. *Adv. Mater.* **2000**, *12*, 333.
(7) Lee, T. M.; Oldenburg, A. L.; Sitafalwalla, S.; Marks, D. L.; Luo, W.; Toublan, F. J. J.; Suslick, K. S.; Boppart, S. A. *Opt. Lett.* **2003**, *28*, 1546.
(8) West, J. L.; Halas, N. J. *Annu. Rev. Biomed. Eng.* **2003**, *5*, 285.
(9) Hirsch, L. R.; Jackson, J. B.; Lee, A.; Halas, N. J.; West, J. *Anal. Chem.* **2003**, *75*, 2377.
(10) Hirsch, L. R.; Stafford, R. J.; Bankson, J. A.; Sershen, S. R.; Rivera, B.; Price, R. E.; Hazle, J. D.; Halas, N. J.; West, J. L. *Proc. Natl. Acad. Sci. U.S.A.* **2003**, *100*, 13549.
(11) Cao, Y. C.; Hua, X. F.; Zhu, X. X.; Wang, Z.; Huang, Z. L.; Zhao, Y. D.; Chen, H.; Liu, M.-X. *J. Immunol. Methods* **2006**, *317*, 163.
(12) Han, M. Y.; Gao, X. H.; Su, J. Z.; Nie, S. *Nat. Biotechnol.* **2001**, *19*, 631.
(13) Siiman, O.; Gordon, K.; Burshteyn, A.; Maples, J. A.; Whitesell, J. K. *Cytometry* **2000**, *41*(4), 298–307.
(14) Ishida, T.; Kuroda, K.; Kinoshita, N.; Minagawa, W.; Haruta, M. *J. Colloid Interface Sci.* **2008**, *323*, 105.
(15) Nath, S.; Ghosh, S. K.; Kundu, S.; Praharaj, S.; Panigrahi, S.; Basu, S.; Pal, T. *Mater. Lett.* **2005**, *59*, 3986.
(16) Vo-Dinh, T. *Trac-Trends in Anal. Chem.* **1998**, *17*, 557.
(17) Kelly, K. L.; Coronado, E.; Zhao, L. L.; Schatz, G. C. *J. Phys. Chem. B* **2003**, *107*, 668.
(18) Ji, T. H.; Lirtsman, V. G.; Avny, Y.; Davidov, D. *Adv. Mater.* **2001**, *13*, 1253.
(19) Oldenburg, S. J.; Jackson, J. B.; Westcott, S. L.; Halas, N. J. *Appl. Phys. Lett.* **1999**, *75*, 2897.
(20) Siiman, O.; Burshteyn, A. *J. Phys. Chem. B* **2000**, *104*, 9795.

Published on Web 11/06/2009

efficient and intense light scattering characteristics of noble metal particles of size ~140 nm or less have enabled their use as fluorescent analogues.[21] By incorporating metal NPs exhibiting preferential scattering characteristics on a polymeric bead surface, the resulting composite microsphere can be used as a scattering contrast agent for biomedical imaging and for labeling cells in flow cytometry.[7,13,20,22−27]

In addition, metal NP-coated polymer beads have been exploited as substrates for SERS.[15,16,28,29] Raman spectroscopy yields an excellent fingerprint of molecules and biological materials, but it suffers from low signal response at concentrations typical of biological systems. The assembly of plasmonic metal (Au and Ag) NPs leads to enhancement of the plasmonic field between the NPs, which in turn leads to shifts in the wavelength and intensity of surface-enhanced plasmon resonance as well as enhancement of the scattered light cross section.[30] Even though different chemistries and shapes of metal NPs, Au spheres,[31] and rods[32] have been used to enhance the SERS, Ag NPs and aggregates have been regarded as the most suitable materials for SERS substrates. This is because Ag gives better enhancement as a result of intense surface plasmon resonance in the visible wavelength, compared with Au.[15,33,34] The SERS effect has broadened the spectrum of possible uses of metal-coated polymer beads for trace chemical analysis and biomedical labeling applications.[35]

A number of recent efforts have focused on fabricating such metal-coated polymer composite beads with tailored structural, optical, and surface properties. These lab-scale processes can be divided roughly into two classes: in-situ (NP grown within polymer) and ex-situ (NP added after formation to polymer) methods. In-situ metal reduction techniques on unmodified PS[1,14,28,29,36−38] or functionalized polymer beads[13,20,29,39−45] have been reported. Unfortunately, irregular and low metal coverage on the beads was typically observed. Additional procedures such as metal ion presoaking,[37] metal seeding,[38] or surface modification[13,20,40,42] are required for higher metal coverage. Nevertheless, it is hard to control the size distribution and aggregation of the metal NPs in the coatings.[1,14,26,36,44−46]

Alternatively, ex-situ techniques for attaching preformed metal NPs with well-defined shape and narrow size distribution to functionalized polymer microspheres have been proposed.[11,47−50] Metal surface coverage less than 30% is usually reported. Electroless plating has been combined with these seeding processes, which led to uniform and dense metallic shells on dielectric core materials.[2,19,51−53] Electrostatic interactions have been utilized in two additional methods: metal NP infiltration into polyelectrolyte-coated beads[18,47,54] and layer-by-layer (LbL) self-assembly.[55−58] In particular, the LbL technique allowed the preparation of a metal layer with uniform and controlled thickness on the polymer beads. However, time-consuming sequential polyelectrolyte deposition cycles and purification steps are required. The assembly may also become unstable in solutions with different pHs or ionic strengths.[59,60] These considerations fuel the demand for alternative methods for the robust incorporation of metal NPs onto polymeric substrates.

Recently, we reported a new method for the preparation of metal NP-coated polystyrene (PS) latex beads: combined swelling−heteroaggregation (CSH).[61] CSH is a facile and relatively benign process that overcomes

(21) Yguerabide, J.; Yguerabide, E. E. *Anal. Biochem.* **1998**, *262*, 137.
(22) Bohmer, R. M.; King, N. J. C. *Cytometry* **1984**, *5*(5), 543–546.
(23) Chen, J.; Saeki, F.; Wiley, B. J.; Cang, H.; Cobb, M. J.; Li, Z. Y.; Au, L.; Zhang, H.; Kimmey, M. B.; Li, X. D.; Xia, Y. *Nano Lett.* **2005**, *5*, 473.
(24) Festin, R.; Bjorklund, B.; Totterman, T. H. *J. Immunol. Methods* **1987**, *101*, 23.
(25) Huang, D.; Swanson, E. A.; Lin, C. P.; Schuman, J. S.; Stinson, W. G.; Chang, W.; Hee, M. R.; Flotte, T.; Gregory, K.; Puliafito, C. A.; Fujimoto, J. G. *Science* **1991**, *254*, 1178.
(26) Siiman, O.; Jitianu, A.; Bele, M.; Grom, P.; Matijevic, E. *J. Colloid Interface Sci.* **2007**, *309*, 8.
(27) Wang, R. K.; Elder, J. B. *Lasers Surg. Med.* **2002**, *30*, 201.
(28) Barnickel, P.; Wokaun, A. *Mol. Phys.* **1989**, *67*, 1355.
(29) Mayer, A. B. R.; Grebner, W.; Wannemacher, R. *J. Phys. Chem. B* **2000**, *104*, 7278.
(30) Michaels, A. M.; Nirmal, M.; Brus, L. E. *J. Am. Chem. Soc.* **1999**, *121*, 9932.
(31) McLaughlin, C.; Graham, D.; Smith, W. E. *J. Phys. Chem. B* **2002**, *106*, 5408.
(32) Nikoobakht, B.; Wang, J. P.; El-Sayed, M. A. *Chem. Phys. Lett.* **2002**, *366*, 17.
(33) Siiman, O.; Lepp, A.; Kerker, M. *Chem. Phys. Lett.* **1983**, *100*, 163.
(34) Tsai, D. P.; Kovacs, J.; Wang, Z. H.; Moskovits, M.; Shalaev, V. M.; Suh, J. S.; Botet, R. *Phys. Rev. Lett.* **1994**, *72*, 4149.
(35) Kim, K.; Lee, H. B.; Park, H. K.; Shin, K. S. *J. Colloid Interface Sci.* **2008**, *318*, 195.
(36) Ou, J. L.; Chang, C. P.; Sung, Y.; Ou, K. L.; Tseng, C. C.; Ling, H. W.; Ger, M. D. *Colloids Surf. A* **2007**, *305*, 36.
(37) Peceros, K. E.; Xu, X. D.; Bulcock, S. R.; Cortie, M. B. *J. Phys. Chem. B* **2005**, *109*, 21516.
(38) Zhang, J. H.; Liu, J. B.; Wang, S. Z.; Zhan, P.; Wang, Z. L.; Ming, N. B. *Adv. Funct. Mater.* **2004**, *14*, 1089.
(39) Chen, C. W.; Chen, M. Q.; Serizawa, T.; Akashi, M. *Chem. Commun.* **1998**, 831.
(40) Chen, C. W.; Serizawa, T.; Akashi, M. *Chem. Mater.* **1999**, *11*, 1381.
(41) Jana, S.; Ghosh, S. K.; Nath, S.; Pande, S.; Praharaj, S.; Panigrahi, S.; Basu, S.; Endo, T.; Pal, T. *Appl. Catal., A* **2006**, *313*, 41.
(42) Jana, S.; Pande, S.; Panigrahi, S.; Praharaj, S.; Basu, S.; Pal, A.; Pal, T. *Langmuir* **2006**, *22*, 7091.
(43) Li, S. N.; Yang, X. L.; Huang, W. Q. *Macromol. Chem. Phys.* **2005**, *206*, 1967.
(44) Liu, W.; Yang, X. L.; Xie, L. *J. Colloid Interface Sci.* **2007**, *313*, 494.
(45) Tamai, H.; Sakurai, H.; Hirota, Y.; Nishiyama, F.; Yasuda, H. *J. Appl. Polym. Sci.* **1995**, *56*, 441.
(46) Liu, W.; Yang, X. L.; Huang, W. Q. *J. Colloid Interface Sci.* **2006**, *304*, 160.
(47) Dokoutchaev, A.; James, J. T.; Koene, S. C.; Pathak, S.; Prakash, G. K. S.; Thompson, M. E. *Chem. Mater.* **1999**, *11*, 2389.
(48) Phadtare, S.; Kumar, A.; Vinod, V. P.; Dash, C.; Palaskar, D. V.; Rao, M.; Shukla, P. G.; Sivaram, S.; Sastry, M. *Chem. Mater.* **2003**, *15*, 1944.
(49) Shi, W. L.; Sahoo, Y.; Swihart, M. T. *Colloids Surf. A* **2004**, *246*, 109.
(50) Westcott, S. L.; Oldenburg, S. J.; Lee, T. R.; Halas, N. J. *Langmuir* **1998**, *14*, 5396.
(51) Kaltenpoth, G.; Himmelhaus, M.; Slansky, L.; Caruso, F.; Grunze, M. *Adv. Mater.* **2003**, *15*, 1113.
(52) Shi, W. L.; Sahoo, Y.; Swihart, M. T.; Prasad, P. N. *Langmuir* **2005**, *21*, 1610.
(53) Yong, K. T.; Sahoo, Y.; Swihart, M. T.; Prasad, P. N. *Colloids Surf. A* **2006**, *290*, 89.
(54) Gittins, D. I.; Susha, A. S.; Schoeler, B.; Caruso, F. *Adv. Mater.* **2002**, *14*, 508.
(55) Cassagneau, T.; Caruso, F. *Adv. Mater.* **2002**, *14*, 732.
(56) Kato, N.; Caruso, F. *J. Phys. Chem. B* **2005**, *109*, 19604.
(57) Liang, Z. J.; Susha, A.; Caruso, F. *Chem. Mater.* **2003**, *15*, 3176.
(58) Liang, Z. J.; Susha, A. S.; Caruso, F. *Adv. Mater.* **2002**, *14*, 1160.
(59) Furusawa, K.; Velev, O. D. *Colloids Surf. A* **1999**, *159*, 359.
(60) Radtchenko, I. L.; Sukhorukov, G. B.; Gaponik, N.; Kornowski, A.; Rogach, A. L.; Mohwald, H. *Adv. Mater.* **2001**, *13*, 1684.
(61) Lee, J. H.; Mahmoud, M. A.; Sitterle, V.; Sitterle, J.; Meredith, J. C. *J. Am. Chem. Soc.* **2009**, *131*, 5048.

Scheme 1. Proposed Combined Swelling−Heteroaggregation (CSH) Process

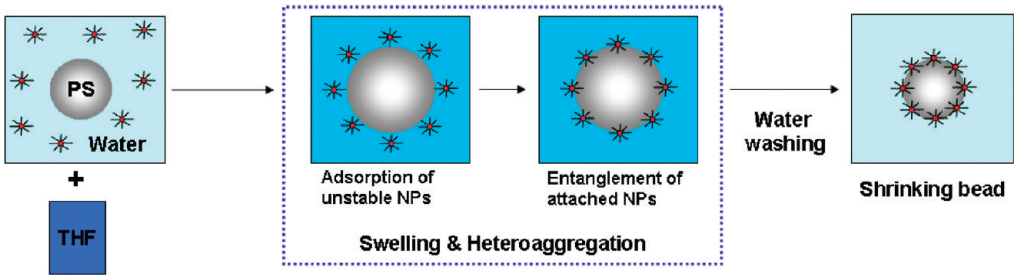

limitations in surface coverage, multistep processing, harsh treatments, and long-term stability concerns of alternative strategies. In the present article, we provide expanded characterization of the process kinetics that allow control over bead optical properties and demonstrate their SERS activity. A range of NPs with different sizes (30, 60, and 80 nm), chemistries (Au and Ag), and shapes (sphere and cube) were successfully coated on unfunctionalized PS beads via CSH, resulting in homogeneous, dense, and stable metal coatings. The kinetics of homo- and heteroaggregation occurring during the CSH process was studied. The metal coverage and morphology and optical properties of the composite beads were controllable by simple adjustments in solvent and NP concentration, chemistry, size, and shape. The optical properties of the resulting metal-coated microspheres were characterized by using dark field microscopy and UV−vis microabsorption spectrometry, and SERS characteristics were studied with Raman spectroscopy.

Experimental Section

Materials. Reagent-grade silver nitrate, hydrogen tetrachloroaurate, sodium citrate, sodium sulfide, poly(vinyl) pyrolidone (PVP, M_n = 55 000 g) and ethylene glycol (EG) were purchased from Aldrich and used as received. Tetrahydrofuran (THF, ≥99.9%) was used as purchased from EMD Chemical Inc. Monodisperse PS microspheres (9.7 μm ± 0.3 μm, 1.0 wt %) in water, cross-linked with 4−8 wt % of divinylbenzene, were obtained from Duke Scientific Corp. Deionized (DI) water (18.2 MΩ cm) was prepared in a Millipore Milli-Q Plus 185 purification system.

Nanoparticle Synthesis. Spherical gold nanoparticles (AuNPs, 32 ± 3 and 79 ± 5 nm, by transmission electron microscopy (TEM)) were prepared by the method of Freund and Spiro[62] with some modification. First, 1 mL hydrogen tetrachloroaurate aqueous solution (0.1 g/10 mL) was added to 100 mL of DI water. Then, the solution was brought to 100 °C. To prepare 30 and 80 nm AuNPs, 2 mL of sodium citrate aqueous solution with concentration of 0.35 and 0.2 g/100 mL were added, respectively, followed by the addition of 0.005 and 0.002 g of PVP, respectively. The resulting solution was stirred at 100 °C for 4 min. The concentrations of the resulting AuNP aqueous solutions were 6.9×10^{11} (30 nm) and 2.9×10^{10} (80 nm) particles mL^{-1}. Silver nanocubes (AgNCs, 62 ± 3 nm, by scanning electron microscopy (SEM)) were prepared by heating 30 mL of EG at 150 °C for 1 h, followed by the addition of a solution of 0.25 g PVP dissolved in 10 mL EG.[63] The resulting solution was heated to return the temperature to 150 °C. Then, 0.4 mL sodium sulfide (3 mM) dissolved in EG was added followed by slow injection of 2.5 mL of 282 mM silver nitrate dissolved in EG. The silver ions were reduced completely after 15 min, producing AgNCs. For purification, the solution was diluted with acetone and DI water and, then, centrifuged at least four times. The particles were then redispersed in DI water at a concentration of 9.7×10^{15} particles mL^{-1}.

Impregnation Step. A 100 μL portion of PS beads aqueous suspension, as-received, was put into a 1.7 mL tube, and 650 μL of the desired metal colloidal dispersion was added and stirred for 30 s. THF was added dropwise to the suspension until the volume percent of THF in water reached 50 vol %, and the mixture was agitated using a rotational shaker for 6 h. The mixture was then washed with DI water via at least four centrifugation cycles. The total mixture volume and amounts of PS and THF were kept constant for all samples. Metal surface coverage was controlled by the ratio of the number of metal NPs to PS particles used in incorporation.

Characterization. UV−vis spectra of metal NPs and composite microbeads in solution were measured with an Ocean optics HR4000Cg-UV-NIR. UV−vis microabsorbance spectra of single metal-coated PS beads were measured using an SEE1100 microspectrometer under 50× magnification. The spot size (3 μm in diameter) was focused onto a single bead. The spectra measured from metal-coated PS beads were referenced to that of a bare PS bead. A Holoprobe Raman microscope (Kaiser Optical Systems) with 785 nm laser excitation was used for surface Raman measurement under 50× magnification. Measurements were done from the $4 \times 4\,\mu m^2$ spot area within a single bead at an accumulation time of 3 s with 15 scans. Dark field optical images were recorded using an inverted Olympus IX70 microscope with a high numerical aperture dark field condenser (U-DCW). SEM was performed with a LEO 1530 instrument for characterizing metal-coated PS beads, and a Zeiss Ultra 60 was used for the AgNCs, respectively. Metal surface coverage on the PS beads was estimated from SEM images using ImageJ software. To measure AuNP size, TEM was performed with a JEOL 100C. Atomic force microscopy (AFM) images of 30 nm AuNP-coated microbeads was obtained using a scanning probe microscope (PicoScan 5, Molecular Imaging) operated in tapping mode with a sharp tip (ACTA, Applied NanoStructures, Inc.).

Results and Discussion

Using the CSH process depicted in Scheme 1, NPs of different sizes (30, 60, and 80 nm), chemistries (Au and Ag), and shapes (sphere and cube) were successfully coated on unfunctionalized PS beads (10 μm in diameter, cross-linked with divinyl benzene), as previously described.[61]

(62) Freund, P. L.; Spiro, M. *J. Phys. Chem.* **1985**, *89*, 1074.
(63) Mahmoud, M. A.; El-Sayed, M. A. *J. Phys. Chem. C* **2008**, *112*, 14618.

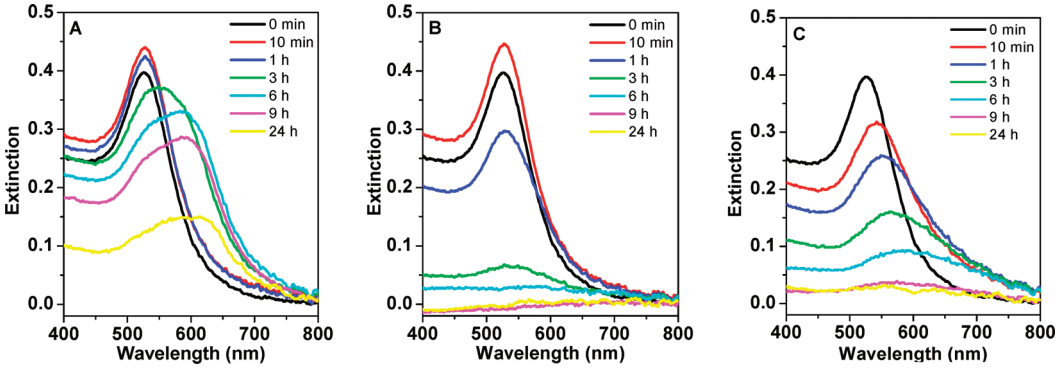

Figure 1. UV−vis spectra of 30 nm AuNPs in THF−water solutions at various times: (A) 50 vol % THF−water solution in the absence of PS beads, (B) 50 vol % THF−water solution in the presence of PS beads, (C) 70 vol % THF−water solution in the absence of PS beads.

Starting with PVP-capped metal NPs and PS beads dispersed in water, homogeneous and dense metal coatings were obtained by the addition and removal of 50 vol % THF, shown in Figure 2A. The process is believed to occur in three steps: (1) THF-induced swelling of the PS beads, (2) heteroaggregation of NPs and PS beads, and (3) deswelling of the beads by removal of THF. On the basis of evidence presented previously,[61] as well as more detailed results below, THF appears to drive the swelling of PS beads and simultaneously induce heteroaggregation of the PVP-capped NPs and PS particles. The resulting composite consists of PS beads covered with metal NPs. The water-dispersed PS beads swell up to 1.5 times their original size and deswell reversibly following the addition and removal, respectively, of 50 vol % THF.[61] Subsequent solvent deswelling likely densifies polymer chains to trap NPs in the polymer outer surface, resulting in dense metal coverage.[61] The integrity of the coatings was verified by UV−vis measurements that showed no observable plasmon peak in supernatant solutions after at least 15 months in water, indicating excellent stability and resistance to metal loss. In addition no evidence of metal loss was observed after 10 min sonication at 50 kHz. These results suggest a strong anchoring of metal NPs on the bead surface that is probably mediated by entanglement of the PVP (from the AuNP surface treatment) with PS. This entanglement likely occurs while the bead is swollen with THF. As the bead is swollen by THF solvent, the polymer matrix becomes liquefied and flexible, facilitating entanglement of the PVP with PS chains.[64,65] Once the THF is removed, the AuNPs are apparently trapped within the glassy PS. Kim et al. proposed a similar mechanism for "grafting" functionalized polymers on PS beads via swelling with an organic solvent followed by shrinking during solvent removal.[65]

Low metal surface coverage (<30%) is a common finding for direct adsorption of metal NPs from aqueous media onto large polymer particles.[47,66] Electrostatic repulsion of capped and charged metallic NPs has proven to be the major difficulty in producing dense coatings.[54] One possible explanation for the dense coating obtained by the CSH technique is an appropriate balance between hetero- and homoaggregation of the PVP-AuNPs and PS particles induced by the addition of a nonsolvent of PVP, THF.

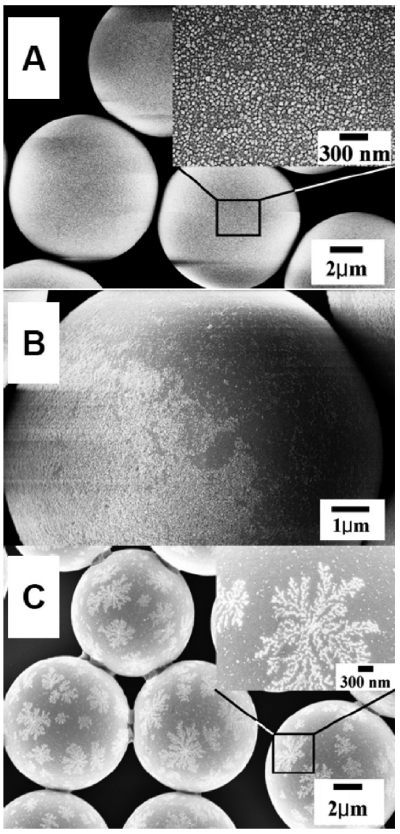

Figure 2. SEM images of 30 nm AuNP-coated PS beads obtained from (A) 50 vol % THF−water solution (n = the ratio of the number of metal NPs to PS particles = 1.3×10^5), (B) 70 vol % THF−water solution ($n = 1.3 \times 10^5$), (C) 50 vol % THF−water solution ($n = 1.0 \times 10^5$).

In order to examine the role of THF in the heteroaggregation, UV−vis spectra of 30 nm AuNPs in 50 vol % THF−water solution were measured at various times, shown in Figure 1A. The plasmon resonance of AuNPs in pure water was indicated by a sharp peak around 526 nm, nearly identical to the "0 min" spectra in Figure 1. After 50 vol % THF was added, the plasmon peak became

(64) Bukowska, A.; Bukowski, W.; Noworol, J. *J. Appl. Polym. Sci.* **2007**, *106*, 3800.
(65) Kim, A. J.; Manoharan, V. N.; Crocker, J. C. *J. Am. Chem. Soc.* **2005**, *127*, 1592.
(66) Caruso, F. *Adv. Mater.* **2001**, *13*, 11.

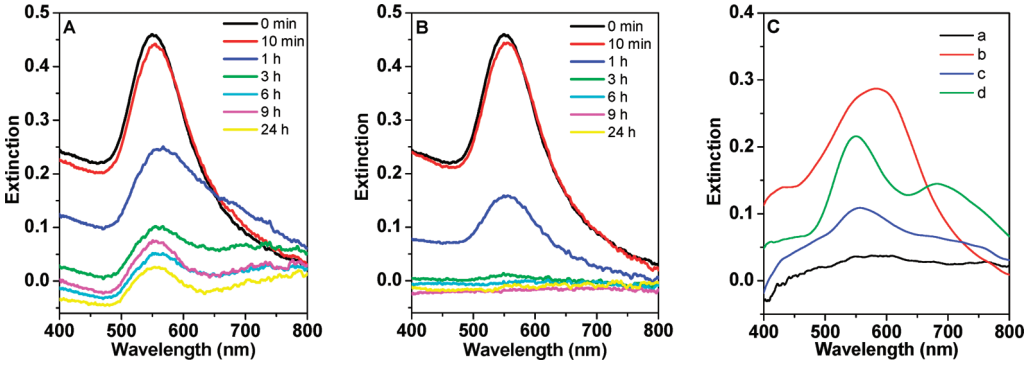

Figure 3. (A and B) UV−vis spectra of 80 nm AuNPs in 50 vol % THF−water solutions at various times: (A) in the absence of PS beads, (B) in the presence of PS beads. (C) UV−vis spectra of AuNP-coated PS beads with different levels of metal coverage dispersed in DI water: (a) 30 nm AuNPs (n = the ratio of the number of metal NPs to PS particles = 1.3×10^5), (b) 30 nm AuNPs ($n = 9.8 \times 10^5$), (c) 80 nm AuNPs ($n = 1.0 \times 10^5$), (d) 80 nm AuNPs ($n = 4.0 \times 10^5$) (The spectra measured from metal-coated PS beads were referenced to that of a plain PS bead.).

increasingly red-shifted, broadened, and decreased in intensity with time after 1 h. These optical phenomena result from the plasmon resonance coupling effect caused by the formation of AuNP aggregates,[67,68] which indicated that the AuNPs were unstable in the 50 vol % THF−water mixture. Significant AuNP aggregation was not observable until after 1 h in the 50 vol % THF−water mixture. The capping polymer, PVP, is readily soluble in water, while it is nearly insoluble in THF.[69−71] Therefore, the effectiveness of PVP as a polymeric stabilizer was diminished and PVP-capped NPs became unstable and aggregated as the composition of THF increased.

Figure 1B shows UV−vis spectra of supernatant solutions that were separated by centrifugation from AuNP−PS cosuspensions in a 50 vol % THF−water mixture at various times. In contrast to Figure 1A, in the presence of PS beads the AuNP plasmon peak showed no red-shifting and minimal broadening over the same time intervals. This result indicated that the homoaggregation of AuNPs in solution was inhibited when PS beads were present. Figure 1B also shows a successive decrease in plasmon peak intensity after 1 and 3 h, indicating disappearance of suspended AuNPs. Together with the SEM evidence (Figure 2A), these results show that the AuNPs heteroaggregate with the swollen PS beads following addition of THF. A clear supernatant solution with no detectable plasmon peak was obtained after 6 h, indicating complete incorporation of AuNPs onto the PS beads.

AuNP homo- and heteroaggregation proceed simultaneously, and heteroaggregate morphology can be controlled by the colloidal stability of the components.[72] We expect that the THF concentration can be used to control the relative stability of the AuNPs and, hence, influence the morphology and deposition speed of the metal coating. THF compositions above 50 vol % led to highly irregular metal coatings, shown in Figure 2B for 70 vol % THF solution. This is thought to be due to homoaggregation of AuNPs occurring prior to heteroaggregation with the PS beads. This was confirmed in Figure 1C, which shows UV−vis spectra of 30 nm AuNPs in 70 vol % THF−water solution at various times. Comparing to the 50 vol % THF solution (Figure 1A), the rate of change (red-shifting, broadening, and decreasing in intensity) of the plasmon peak became faster, and the plasmon resonance peak disappeared entirely after 9 h. This result indicates that at 70 vol % THF the rate of AuNP homoaggregation was apparently much faster than the heteroaggregation of AuNPs and PS beads, compared to 50% THF. Significant homoaggregation interferes with the formation of a continuous metal particle coating (Figure 2B). In contrast, at THF compositions lower than 50 vol %, AuNPs were stable, leading to PS beads with less metal coating. In fact, no deposition of AuNPs was observed for THF concentrations less than 25 vol % even after 24 h, which was verified by the white color of the resulting beads.

UV−vis spectra of 80 nm AuNPs in THF−water solution showed results similar to those of 30 nm AuNPs, shown in Figure 3A and B. In the absence of PS, the AuNPs homoaggregated upon addition of 50 vol % THF with a broad plasmon resonance peak at long wavelength developing (Figure 3A). A broad plasmon band at long wavelengths originates from interparticle plasmon field coupling due to the formation of AuNP homoaggregates. However, in the presence of PS beads, the AuNPs heteroaggregated with the PS particles, resulting in no detectable broad peak at long wavelength in the supernatant solution over the same time intervals (Figure 3B).

Bead shrinkage, induced by the removal of THF via water washing, resulted in a densification of the metal NP coating on the PS beads. The mechanism of deswelling and densification can alter significantly the morphology of NP assemblies on the PS beads. For example, a dendritic morphology of AuNPs was observed at the specific range of NP loading ($0.7 \times 10^5 < n$ (the ratio of the number of metal NPs to PS particles) $< 1.3 \times 10^5$), shown in Figure 2C. Nonequilibrium dendritic patterns of metal NPs are known to form at flat interfaces under

(67) Lazarides, A. A.; Kelly, K. L.; Jensen, T. R.; Schatz, G. C. *J. Mol. Struct.-Theochem* **2000**, *529*, 59.
(68) Lazarides, A. A.; Schatz, G. C. *J. Phys. Chem. B* **2000**, *104*, 460.
(69) Graf, C.; Vossen, D. L. J.; Imhof, A.; van Blaaderen, A. *Langmuir* **2003**, *19*, 6693.
(70) Qian, W. X.; Xing, R. B.; Yu, X. H.; Quan, X. J.; Han, Y. C. *J. Chem. Phys.* **2007**, *126*, 064901.
(71) Smith, J. N.; Meadows, J.; Williams, P. A. *Langmuir* **1996**, *12*, 3773.
(72) Wang, G. H.; Nicholson, P. S. *J. Am. Ceram. Soc.* **2001**, *84*, 1250.

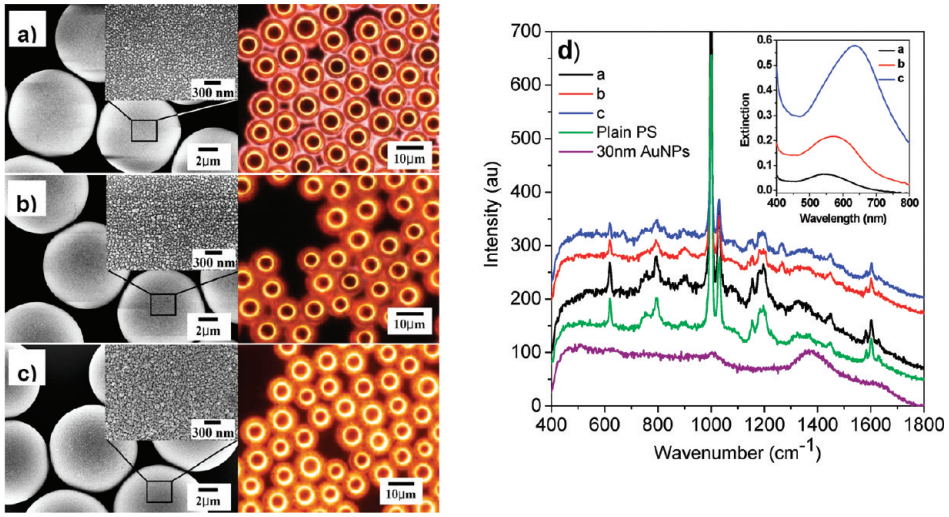

Figure 4. SEM (left) and dark field (right) images (a−c) and surface-enhanced Raman spectra (d) and the corresponding UV−vis spectra (d, inset) of 10 μm PS beads coated by 30 nm AuNPs with different levels of metal coverage: (a) n = the ratio of the number of metal NPs to PS particles = 1.3×10^5, (b) $n = 2.5 \times 10^5$, (c) $n = 9.8 \times 10^5$. (UV−vis spectra were measured from of a single PS bead covered by AuNPs and obtained by subtracting that of a plain PS bead to see altered optical properties of the PS beads by metal coating.)

appropriate diffusion-controlled conditions.[73−76] NP dendrites have been observed to form in the presence of polymer stabilizers such as PVP, as well as small molecule promoters such as pyridine.[73,75] Nonequilibrium dendritic structure formation is often observed to be sensitive to preparatory conditions, such as particle concentrations, which appears to be the case in the present study.[74] Under diffusion-limited aggregation, an optimum concentration is observed because high NP concentrations lead to particles being too closely compacted and low NP concentrations supply insufficient numbers of NPs for building dendritic structures. The effect of substrate curvature on dendrite formation via diffusion-limited aggregation is not known. However, the large PS beads have relatively low curvature compared to the NPs and represent a close approximation to a flat surface.

The fraction of AuNPs should be useful as a parameter for adjusting surface coverage. Figure 3C shows UV−vis spectra of 30 and 80 nm AuNP-coated PS beads with different NP concentrations dispersed in DI water. The plasmon resonance peak appeared around 560 nm at the lowest metal surface coverage for the 30 nm AuNP coated-PS beads (curve a of Figure 3C). This peak was red-shifted by ~30 nm, compared to that of the individual AuNPs dispersed in DI water. The red-shift of the peak can be related to (1) the change in the local dielectric of the surrounding medium that occurs after deposition of AuNPs on the PS bead surface and (2) interparticle plasmon field coupling resulting from densification of NPs on the PS surface.[77] The plasmon peak became further red-shifted to ~590 nm and increased in intensity as NP concentration increased (curve b of Figure 3C). This is due to increased interparticle plasmon field coupling associated with the increase of the metal coverage on the beads.[77] For the PS beads covered by 80 nm AuNPs, a single broad plasmon peak (~555 nm) was observed for the lowest NP concentration (curve c of Figure 3C). However, another broad plasmon peak appeared at longer wavelengths (~ 690 nm) and increased in intensity with the higher NP fraction (curve d of Figure 3C). The increase in intensity of the surface plasmon resonance peak at ~550 nm, corresponding to isolated AuNPs, is due to increasing numbers of relatively isolated AuNPs on the bead surface. The appearance of an additional low energy resonance peak at 690 nm is attributed to the onset aggregation of AuNPs on the polymer bead with higher metal coverages. These results were consistent with SEM images and UV−vis microabsorption spectra of single beads, described below.

Figures 4a−c show SEM and dark field optical microscope images of the 30 nm AuNP-coated PS beads at different metal coverages. Metal surface coverage increased (reaching a maximum total surface coverage of 89%) as NP concentration increased, shown in Figure 4c. Dark field images demonstrated that brightness increased as metal surface coverage increased (Figure 4a−c). Detailed surface morphology of the metal coating on the bead was examined by AFM images. Overall, the metal coating was homogeneous and relatively smooth without any large clumps of NPs (Figure 5A). AFM images also indicated that the 30 nm AuNP coating consisted of 1 to ~3 dense NP layers, shown in Figure 5B.

To characterize the optical properties of NP-coated PS beads, UV−vis spectra from single beads covered with 30 nm AuNPs were measured, shown in the inset of Figure 4d. The plasmon resonance peak was red-shifted from 545 to 650 nm and significant increases in intensity and broadening of the plasmon resonance peak were observed as metal surface coverage increased (curves a−c of Figure 4d, inset). The position, intensity, and

(73) Agrawal, V. V.; Kulkarni, G. U.; Rao, C. N. R. *J. Colloid Interface Sci.* **2008**, *318*, 501.
(74) Corno, J. A.; Stout, J.; Yang, R.; Gole, J. L. *J. Phys. Chem. C* **2008**, *112*, 5439.
(75) Jin, Y. D.; Dong, S. J. *Angew. Chem., Int. Ed.* **2002**, *41*, 1040.
(76) Sander, L. M. *Nature* **1986**, *322*, 789.
(77) Jiang, C. Y.; Markutsya, S.; Tsukruk, V. V. *Langmuir* **2004**, *20*, 882.

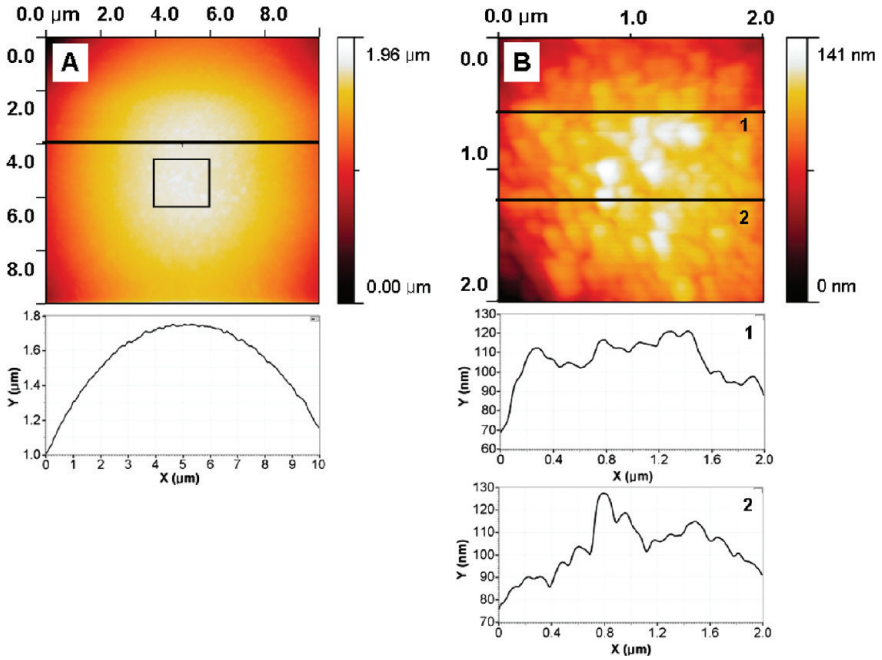

Figure 5. AFM surface images (top) of a PS bead covered by 30 nm AuNPs (corresponding Figure 4c) and line profiles along the line (bottom) on the AFM images: (a) single bead ($10 \times 10\ \mu m^2$), (b) boxed area of bead in (A) ($2 \times 2\ \mu m^2$).

broadening of the plasmon resonance of the metal NP assembly can be explained qualitatively by Mie scattering theory, which accounts for the dependence of the plasmon resonance on particle size and shape, the surrounding dielectric environment, and interparticle distance.[77−81] Closely packed metal NP assemblies have been achieved on planar[77,79,80,82,83] and spherical surfaces.[18,37,38] The overall plasmon resonance band of the highly packed metal NP assembly consists of concurrent individual and interparticle coupling plasmon resonance at long wavelength, which depends strongly on interparticle spacing.[77,79,80] Because of nonuniformity of interparticle separation distribution, a single broad resonance peak, resulting from a superimposition of both individual and interparticle collective surface plasmon resonance has been observed usually. The red-shift and increase in intensity of the plasmon peak is due predominantly to the interparticle collective resonance.[77] Hence, significant red-shifting and broadening of the surface plasmon resonance band with an increase of metal coverage on the PS bead surface is attributed to intensified interparticle coupling resonance due to AuNP crowding on the PS beads. This result is consistent with other work, where the red-shift of the plasmon peak position from 520−560 to 650−660 nm was observed as the AuNP density increased on planar surfaces.[77,80,83] As for AuNP assemblies on the spherical surface, a broad and red-shifted resonance at 660 nm was predicted for a nanoshell composed of 30 nm AuNPs by using a discrete dipole approximation model.[37] Other experimental works have shown that complete metal shells on PS beads showed a broad and red-shifted plasmon peak around 680 nm.[18,38] The spectra (curve c of Figure 4d, inset) of 30 nm Au coated beads with the highest coverage from this work showed a similar plasmon resonance wavelength as complete Au shells. Figure 4d shows the SERS spectra of 30 nm AuNPs and PS beads coated with different amounts of 30 nm AuNPs. For the AuNP-PS composite beads, all the expected Raman bands of PS appeared at 1014, 1210, and 633 cm^{-1}, assigned to phenyl ring breathing and radial ring stretching modes. The bands at 1196 and 1170 cm^{-1}, corresponding to CH in-plane bending modes,[84] are less intense compared with those of plain PS beads, and their intensities were found to decrease as the amount of AuNP coating increased. This is due to a decrease in the exposed PS area, as the surface became more coated with metal. Since the NPs on the PS surface shield the surface from the Raman laser, a minimal Raman band corresponding to the PS was detected when the surface was completely coated by NPs.[35] In contrast, the degree of enhancement in the vibration bands of the pyrrolidone ring of PVP increased as the metal coverage increased: 571 cm^{-1} (C═O bending), 667 cm^{-1} (N—C═O ring deformation), 821 cm^{-1} (C—C bond vibration of the ring), 895 cm^{-1} (ν(C—C) ring breathing), and 1265 cm^{-1} (CH_2 ring wagging). The surface plasmon resonance field emanating from the metal NP assembly is responsible for the enhancement in PVP Raman signals, compared to the

(78) Averitt, R. D.; Sarkar, D.; Halas, N. J. *Phys. Rev. Lett.* **1997**, *78*, 4217.
(79) Jiang, G. Q.; Baba, A.; Ikarashi, H.; Xu, R. S.; Locklin, J.; Kashif, K. R.; Shinbo, K.; Kato, K.; Kaneko, F.; Advincula, R. *J. Phys. Chem. C* **2007**, *111*, 18687.
(80) Malikova, N.; Pastoriza-Santos, I.; Schierhorn, M.; Kotov, N. A.; Liz-Marzan, L. M. *Langmuir* **2002**, *18*, 3694.
(81) Mie, G. *Ann. Phys.* **1908**, *25*, 377.
(82) Bhat, R. R.; Genzer, J.; Chaney, B. N.; Sugg, H. W.; Liebmann-Vinson, A. *Nanotechnology* **2003**, *14*, 1145.
(83) Bhat, R. R.; Tomlinson, M. R.; Genzer, J. *Macromol. Rapid Commun.* **2004**, *25*, 270.
(84) Compagnini, G.; Pignataro, B.; Pelligra, B. *Chem. Phys. Lett.* **1997**, *272*, 453.

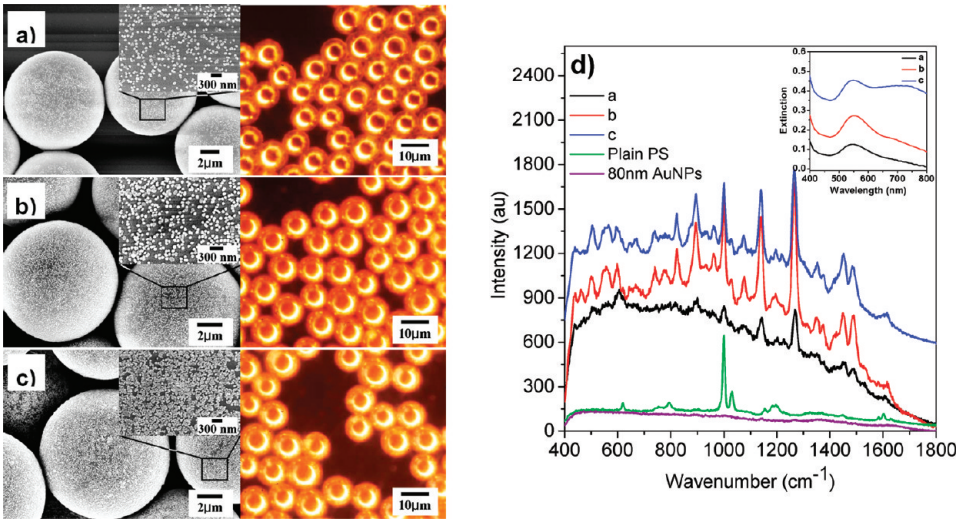

Figure 6. SEM (left) and dark field (right) images (a−c) and surface-enhanced Raman spectra (d) and the corresponding UV−vis spectra (d, inset) of 10 μm PS beads coated by 80 nm AuNPs with different levels of metal coverage: (a) $n = 1.0 \times 10^5$, (b) $n = 2.0 \times 10^5$, (c) $n = 4.0 \times 10^5$. (UV−vis spectra were measured from of a single PS bead covered by AuNPs and obtained by subtracting that of a plain PS bead to see altered optical properties of the PS beads by metal coating.)

very weak Raman signal of bulk PVP.[35,85] Raman signal intensities increase as the plasmon resonance intensity of the NPs at the Raman excitation wavelength increases, shown in Figure 4d.[78]

For the 80 nm AuNP-coated PS beads, metal coverage on the bead was also proportional to the concentration of NPs used. From SEM images of 80 nm AuNP-coated PS beads, the surface coverage continued to increase from approximately 27% to 63% as AuNP concentration increased (Figures 6a−c). At the lowest metal coverage, individual AuNPs were observed uniformly without any AuNP aggregation on the beads (Figure 6a). As the metal coverage increased, interparticle distance decreased and AuNPs started to form aggregates on the surface, resulting an increase in surface roughness (Figure 6b). The maximum number of AuNP aggregates on the PS beads, and the highest surface roughness, was observed at the highest metal coverage (Figure 6c). Dark field images of the PS beads covered with 80 nm AuNPs were brighter than those of 30 nm AuNP-coated PS beads, in spite of lower metal coverage. This is due to the higher scattering power of the larger sized AuNPs. For all particle sizes, higher surface coverage resulted in brighter images in dark field microscopy.

A surface plasmon band with one peak around 545 nm was observed for the 80 nm AuNP-coated PS bead with the lowest metal coverage, illustrated in the inset of Figure 6d (curve a). A strong and sharp extinction peak (~545 nm) is due to the plasmon resonance of individual AuNPs on the PS bead surface. At higher metal coverage, another broad peak appeared at longer wavelength around 680 nm, and it continued to become further intensified, broadened, and red-shifted to 740 nm (curves b and c of Figure 6d, inset) as metal coverage increased. This low energy resonance peak is attributed to the interparticle coupling resonance which depends strongly on interparticle distance.[77,80] Increasing metal coverage and the AuNP aggregation on the beads caused enhanced interparticle plasmon coupling and further red-shifting (from 680 to 740 nm), broadening, and intensification of the peak. On the other hand, the intensity of the individual plasmon peak (~545 nm) increased monotonically without red-shifting as the metal coverage increased. This result indicates the dominant effect of interparticle coupling resonance on the red-shift of the resonance band at higher metal density in the AuNP assembly.[77] UV−vis spectra were consistent with the morphology of the AuNP coating verified from SEM (Figures 6a−c). For slightly bigger nanoparticles (>30 nm), enhancement in the SERS spectra of PVP increases as the NP size increases, due to the increase of the surface plasmon field. Figure 6d shows the SERS spectra of 80 nm AuNPs and PS beads coated with 80 nm AuNPs. As the large AuNPs scatter incident light away from the surface of PS, fewer photons are scattered from the surface of PS and less Raman photons corresponding to PS are generated as AuNP coverage increases. Therefore, most of the Raman bands corresponding to the PS disappeared or weakened. On the other hand, all Raman bands corresponding to the PVP are enhanced by the stronger plasmon field due to the increased metal coverage.[35] The composite bead with moderate metal coverage (Figure 6b and curve b of Figure 6d) showed more enhanced Raman signals than the bead with the lowest metal coverage (Figure 6a and curve a of Figure 6d), because the plasmon peak intensity of the denser metal coating is stronger at the excitation line (785 nm). Although the AuNP-coated bead with the highest metal coverage (curve c of Figure 6d) has the strongest plasmon peak at the excitation frequency, the SERS bands are less intense than those of the moderate metal coverage (curve b of Figure 6d). SEM images indicated the surface roughness of the metal-coated beads increased due to the formation of aggregates of AuNPs on the beads as the

(85) Mahmoud, M. A.; Tabor, C. E.; El-Sayed, M. A. *J. Phys. Chem. C* **2009**, *113*, 5493.

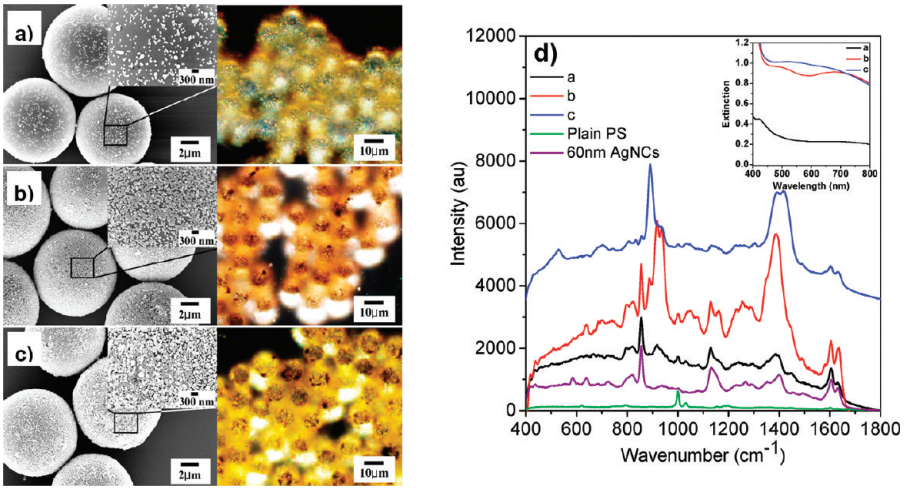

Figure 7. SEM (left) and dark field (right) images (a–c) and surface-enhanced Raman spectra (d) and the corresponding UV–vis spectra (d, inset) of 10 μm PS beads coated by 60 nm AgNCs with different levels of metal coverage: (a) $n = 1.0 \times 10^9$, (b) $n = 2.0 \times 10^9$, (c) $n = 3.5 \times 10^9$. (UV–vis spectra were measured from of a single PS bead covered by AgNCs and obtained by subtracting that of a plain PS bead to see altered optical properties of the PS beads by metal coating.)

metal coverage increased. However, AuNP aggregates formed larger clusters on the bead surface at the highest metal coverage (Figure 6c). Hence, a decrease in the intensity of SERS bands at the highest metal coverage might be due to destructive interference between the Raman photons generated in high aggregation areas.[86]

Silver nanocubes (AgNCs) (60 nm, cube) were also successfully coated on the polymer beads using the CSH technique. Aqueous suspensions of the AgNC-coated beads exhibited various colors ranging from intense yellow, brown, and gray to black as the AgNC concentration increased. Figures 7a–c show SEM and dark field images of the 60 nm AgNC-coated PS beads as a function of metal coverage. Metal surface coverage ranged from 16% to 82% with some AgNC aggregations. Even with low surface coverage, bright images of AgNC-coated PS beads were observed in dark field microscopy due to the highly scattering nature of cubic AgNCs (Figure 7a). Compared to the single AgNC plasmon bands that scatter blue light, the AgNC aggregate plasmon peak scatters red light.[85] Hence, as AgNC coverage on the beads increased, the amount of red light observed in the dark field image increased and the dominant scattered color changed from blue to red (Figure 7a and b), indicating an increased number of aggregates. At the highest metal coverage, the dark field image of the composite beads showed yellow color (Figure 7c), indicating a higher degree of aggregation into clusters that scatter yellow light. Corresponding SEM images (Figures 7a–c) supported the results of dark field images well.

The morphology of the AgNC metal coatings corresponded well with single bead UV–vis microabsorption spectra. The plasmon resonance peak of the PS bead coated with 60 nm AgNCs appeared at about 420 nm (curve a of Figure 7d, inset), which originates from individual plasmon resonance. For higher Ag coverage, the plasmon resonance peak became red-shifted to around 480 nm, with a broad peak at long wavelength (~690 nm) appearing (curve b of Figure 7d, inset). A significant increase in the scattering intensity and the broadening of the plasmon resonance were observed at the highest metal coverage (curves c of Figure 7d, inset), resulting in a single plasmon peak. The broadening, red-shifting, and development of long wavelengths of the plasmon spectrum with highly enhanced scattering is again explained by the intensified interparticle coupling effect due to crowded AgNCs and increased aggregation of AgNCs on the bead surface, shown in Figure 7b and c. Figure 7d shows the SERS spectra of 60 nm AgNCs and AgNC-coated PS beads with different levels of metal coverage. The SERS bands of PVP in the case of pure AgNCs are more intense than spherical AuNPs. This could be due to a higher concentration of capping PVP molecules on the AgNCs as well as the more intense plasmon field of the Ag cubic shape relative to the spherical AuNPs. The degree of SERS enhancement of the bands corresponding to PVP of AgNC-coated beads with the lowest metal coverage is the smallest because the plasmon peak around the laser excitation line is weak (curve a of Figure 7d). On the other hand, the composite bead with moderate Ag coverage has the highest SERS enhancement, because the gap distance decreases and the plasmon coupling between the particles becomes stronger (curve b of Figure 7d). However, in the case of the highest surface coverage, a higher degree of aggregation into clusters with increased roughness was observed in the SEM and dark field images (Figure 7c). Randomly arranged AgNC assemblies could cause destructive interference of Raman photons generated with different modes and, hence, decrease the SERS intensity of the composite bead with the highest Ag coverage (curve c of Figure 7d).[86]

Conclusions

In summary, noble metal (Au or Ag)-coated PS latex beads have been prepared by a solvent (THF)-controlled

(86) Kim, K.; Lee, H. S.; Kim, N. H. *Anal. Bioanal. Chem.* **2007**, *388*, 81.

CSH technique. Different sizes (30, 60, and 80 nm), chemistries (Au and Ag), and shapes (sphere and cube) of NPs can be coated on commercially available, unfunctionalized PS beads, resulting in dense and uniform metal coatings on the beads. The resulting composite microspheres were stable and showed no loss of the metal coating during long-term (15 months) water storage.

THF appears to play two major roles in this technique: (1) as a solvent of PS, it plasticizes the PS surface during swelling, allowing entanglement with the PVP present on the metal NPs, and (2) as a nonsolvent of PVP, it induces the heteroaggregation and adsorption of PVP-capped metal NPs on PS and allows control over the resulting morphology and surface coverage by driving instability of the NPs in the THF−water mixture.

To achieve a homogeneous metal coating, it was crucial to control the relative rate of homo- and heteroaggregation of particles by adjusting THF concentration, so that the PS beads and NPs heteroaggregate while avoiding their homoaggregation. The morphology and surface coverage of the metal coating on the beads, and thus the optical properties, were effectively controlled by adjusting the THF and NP concentrations as well as the NP chemistry, shape, and size. Continuous and close-packed metal coatings, with optical properties similar to complete shells, were obtained with smaller and spherical AuNPs. For the larger AuNPs or cubic AgNCs, less dense metal coatings were achieved, but they showed higher scattering properties due to the particles' inherent highly scattering nature. The metal-coated beads were characterized as SERS substrates by using Raman spectroscopy. It was shown that the AgNC-coated polymer beads were the most effective SERS substrates, exhibiting highly enhanced Raman signals of PVP capping molecules.

The resulting metal coated-polymer microspheres are of interest for applications in biomedical imaging, sensors, photonics, SERS, and electronics. In addition, the CSH technique is a facile and relatively benign single-step process.

Acknowledgment. The authors would like to thank Prof. M. A. El-Sayed for useful discussions and Lance Rodeman and Megan Mackey for assisting with experiments. We also thank Prof. M. Srinivasarao for the use of UV−vis microspectrometer facilities. This work was partially supported by KaVo Dental Corp, GmbH, and the NSF (grant no. 3306FJ9).

Supporting Information Available: TEM and SEM images of metal nanoparticles used in the present study (PDF). This material is available free of charge via the Internet at http://pubs.acs.org.